AD

FREE-PISTON ENGINE LINEAR GENERATOR FOR HYBRID VEHICLES MODELING STUDY

INTERIM REPORT
TFLRF No. 305

By

T.J. Callahan
Engine and Vehicle Research Division
Southwest Research Institute
San Antonio, Texas

and

S.K. Ingram
UT/Center for Electromechanics
The University of Texas at Austin
Austin, Texas

"Original contains color plates: All DTIC reproductions will be in black and white"

Under Contract to

U.S. Army TARDEC
Mobility Technology Center–Belvoir
Fort Belvoir, Virginia

Prepared for

Advanced Research Projects Agency
Arlington, Virginia 22203-1714

Contract No. DAAK70-92-C-0059

Approved for public release; distribution unlimited

May 1995

Disclaimers

The findings in this report are not to be construed as an official Department of the Army position unless so designated by other authorized documents.

Trade names cited in this report do not constitute an official endorsement or approval of the use of such commercial hardware or software.

DTIC Availability Notice

Qualified requestors may obtain copies of this report from the Defense Technical Information Center, Cameron Station, Alexandria, Virginia 22314.

Disposition Instructions

Destroy this report when no longer needed. Do not return it to the originator.

DISCLAIMER NOTICE

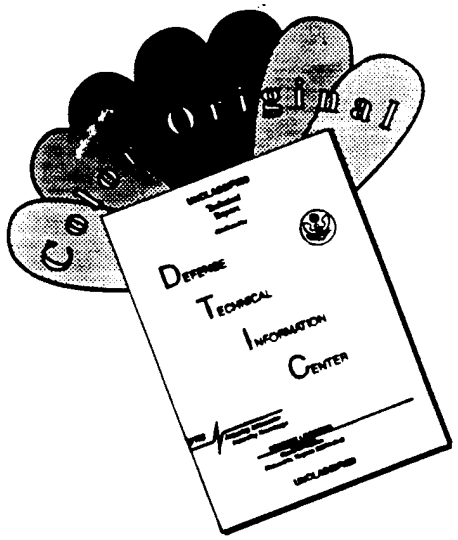

THIS DOCUMENT IS BEST QUALITY AVAILABLE. THE COPY FURNISHED TO DTIC CONTAINED A SIGNIFICANT NUMBER OF COLOR PAGES WHICH DO NOT REPRODUCE LEGIBLY ON BLACK AND WHITE MICROFICHE.

REPORT DOCUMENTATION PAGE

Form Approved
OMB No. 0704-0188

1. AGENCY USE ONLY (Leave blank)	2. REPORT DATE	3. REPORT TYPE AND DATES COVERED
	May 1995	Interim January 1994 to August 1994

4. TITLE AND SUBTITLE

Free Piston Engine Linear Generator for Hybrid Vehicles Modeling Study

5. FUNDING NUMBERS

DAAK70-92-C-0059; WD 20

6. AUTHOR(S)

Callahan, T.J. and Ingram, S.K.

7. PERFORMING ORGANIZATION NAME(S) AND ADDRESS(ES)

Southwest Research Institute
P.O. Drawer 28510
San Antonio, Texas 78228-0510

UT/Center for Electromechanics
The University of Texas
Austin, Texas

8. PERFORMING ORGANIZATION REPORT NUMBER

TFLRF No. 305

9. SPONSORING/MONITORING AGENCY NAME(S) AND ADDRESS(ES)

Department of the Army
Mobility Technology Center-Belvoir
10115 Gridley Road, Suite 128
Ft. Belvoir, Virginia 22060-5843

Advanced Research Projects Agency
3701 N. Fairfax Drive
Arlington, Virginia 22203-1714

10. SPONSORING/MONITORING AGENCY REPORT NUMBER

11. SUPPLEMENTARY NOTES

12a. DISTRIBUTION/AVAILABILITY STATEMENT

Approved for public release; distribution unlimited

12b. DISTRIBUTION CODE

13. ABSTRACT (Maximum 200 words)

Development of a free piston engine linear generator was investigated for use as an auxiliary power unit for a hybrid electric vehicle. The main focus of the program was to develop an efficient linear generator concept to convert the piston motion directly into electrical power. Computer modeling techniques were used to evaluate five different designs for linear generators. These designs included permanent magnet generators, reluctance generators, linear DC generators, and two- and three-coil induction generators. The efficiency of the linear generator was highly dependent on the design concept. The two-coil induction generator was determined to be the best design, with an efficiency of approximately 90 percent.

14. SUBJECT TERMS

Free Piston Engine
Generator
Auxiliary Power Unit
Linear Generator
Modeling

15. NUMBER OF PAGES

45

16. PRICE CODE

17. SECURITY CLASSIFICATION OF REPORT	18. SECURITY CLASSIFICATION OF THIS PAGE	19. SECURITY CLASSIFICATION OF ABSTRACT	20. LIMITATION OF ABSTRACT
Unclassified	Unclassified	Unclassified	

EXECUTIVE SUMMARY

Problems and Objectives: The objective of this program was to evaluate the feasibility of using a free piston engine (FPE) coupled to a linear generator (LG) as an auxiliary power unit (APU). The current application for the APU is in providing peak shaving power and recharging batteries on a hybrid electric vehicle. The main challenge in developing a successful FPELG is to develop an efficient linear generator to convert the piston motion directly into electrical power.

Importance of Project: Environmental regulations on air quality and vehicle exhaust emissions are placing severe restrictions on vehicles powered with traditional automotive engines. Hybrid electric vehicles potentially can approach a zero emission vehicle if only the vehicle is considered. The deficiencies with electric vehicles include limited driving range, weight and size of the batteries, and the time to refill or charge the batteries. The addition of an APU to an electric vehicle addresses these deficiencies.

Technical Approach: In this program, computer-modeling techniques were used to evaluate different designs for the linear generator. A computer model of a FPE was used to determine typical piston velocity profiles. The velocity profiles were used as design input for designing and modeling linear generators. The models were used to predict voltage and current profiles and also generator efficiency.

Accomplishments: Five different linear generator designs were evaluated. These designs included permanent magnet generators, reluctance generators, linear DC generators, and two- and three-coil induction generators. The efficiency of the linear generator was highly dependent on the design concept. The two-coil induction generator was determined to be the best design with an efficiency of approximately 90 percent.

Military Impact: An APU has many military applications. A FPELG can offer a compact, mechanically simple design for an APU that can be man-portable or vehicle distributed. Because the piston is not constrained by a connecting rod, the engine can achieve variable compression ratios, making it adaptable to a wide range of fuels, including JP-4, JP-8, natural gas, diesel fuels, and other potential alternative fuels.

FOREWORD

This work was performed by Southwest Research Institute (SwRI), San Antonio, TX and the University of Texas at Austin during the period January 1994 through August 1994 under Contract No. DAAK70-92-C-0059. The work was funded by the U.S. Army TARDEC Mobility Technology Center-Belvoir (MTCB), Ft. Belvoir, VA. Mr. T.C. Bowen (AMSTA-RBFF) of MTCB served as the contracting officer's representative. Major Rick Cope of the Advanced Research Projects Agency served as the project technical monitor.

TABLE OF CONTENTS

LIST OF ILLUSTRATIONS

LIST OF ABBREVIATIONS

ARPA	Advanced Research Projects Agency
APU	Auxiliary Power Unit
ZEV	Zero-emission Vehicle
HEV	Hybrid Electric Vehicle
FPE	Free Piston Engine
LG	Linear Generator
BDC	Bottom Dead Center
TDC	Top Dead Center
DC	Direct Current
UT/CEM	University of Texas/Center for Electromechanics
SwRI	Southwest Research Institute
EM	Electromechanics
FEM	Finite Element Modeling
A	Amperes
T	Tesla
V	Volts
Ω	Ohms
J	Joules
Hz	Hertz
N	Newtons

I. INTRODUCTION

Environmental regulations on air quality and vehicle exhaust emissions are placing severe restrictions on vehicles powered with traditional automotive engines. An alternative to the traditional vehicle is the electric vehicle. Electric vehicles potentially can approach a zero emission vehicle (ZEV) if one considers only the vehicle. However, difficulties with electric vehicles that must be considered include limited driving range, weight and size of the batteries, and the time required to refill or recharge the batteries. Hence, the Advanced Research Projects Agency (ARPA) has been focusing research on Hybrid Electric Vehicles (HEV), an electric vehicle with an auxiliary power unit (APU). In this context, the APU can be any engine capable of providing power for driving or recharging the batteries.

The addition of an APU to an electric vehicle addresses the previously mentioned difficiencies. By using an APU in conjunction with the batteries, several benefits are derived. These benefits include the following: (1) the driving range of the vehicle can be extended; (2) power provided by the APU during peak demand can supplement the maximum power supplied by the batteries, resulting in smaller batteries; and (3) the APU can be used to recharge the batteries while the vehicle is being driven, reducing or eliminating the time required for recharging while the vehicle is out of service.

Several desirable characteristics of an APU for HEV applications include the following: (1) the APU must generate electric power for peak power demand and battery recharging; (2) the APU must be compact with a high power-to-weight ratio; (3) the APU must have a high efficiency with low exhaust emissions, and (4) considering that the APU is not the prime mover of the vehicle, the APU must be inexpensive to manufacture and it must be reliable.

These characteristics are obviously desirable of all engines. There are many combinations of engines and alternators/generators that could be used as an APU. This report addresses the use of a free-piston engine (FPE) coupled with a linear generator (LG) as a potential APU for HEVs. FPEs are engines that produce power or work without the benefit of a crankshaft for power output. FPE have been produced commercially, but without much market success since the

1930s. FPEs have been used as air or natural gas compressors (Fig. 1) (1-6)* and they have also been proposed for use as hydraulic pumps (Fig. 2) (7-10). In both these modes, the power is extracted directly from the piston by performing work on a second fluid. A linear generator can also be used to extract power directly from the piston (Fig. 3) by converting the piston motion into electrical energy.

When compared to a conventional reciprocating engine, a FPELG has the following potential advantages:

- Mechanically simple – The piston is the only moving part of a FPE.

- Reduced wear – Since the generator acts directly on the piston, there are only limited side thrust forces that are typical of the conventional engine. There are also no bearings required for crankshafts.

- Inherently balanced – If an opposed piston arrangement is used for the design, the engine will be inherently balanced.

- Variable compression ratio – The piston is not constrained by mechanical linkages. This it can vary its stroke to obtain compression ratios higher than conventional engines and can be adjusted for fuel quality and maximum efficiency.

The challenge in developing a successful FPELG is overcoming several potential technical disadvantages. The primary objective is to develop an efficient linear generator to convert the piston motion into electrical power. A secondary goal is to maintain control of the engine. Conventional engines use crankshaft position sensors to time spark and fuel injection events. Without a crankshaft, the FPE controls will have to sense and perhaps control the piston motion to produce an efficient thermodynamic cycle. With the computer and controls technology available, sensing and controlling the piston position may be achieved.

* Underscored numbers in parentheses refer to the list of references at the end of this report.

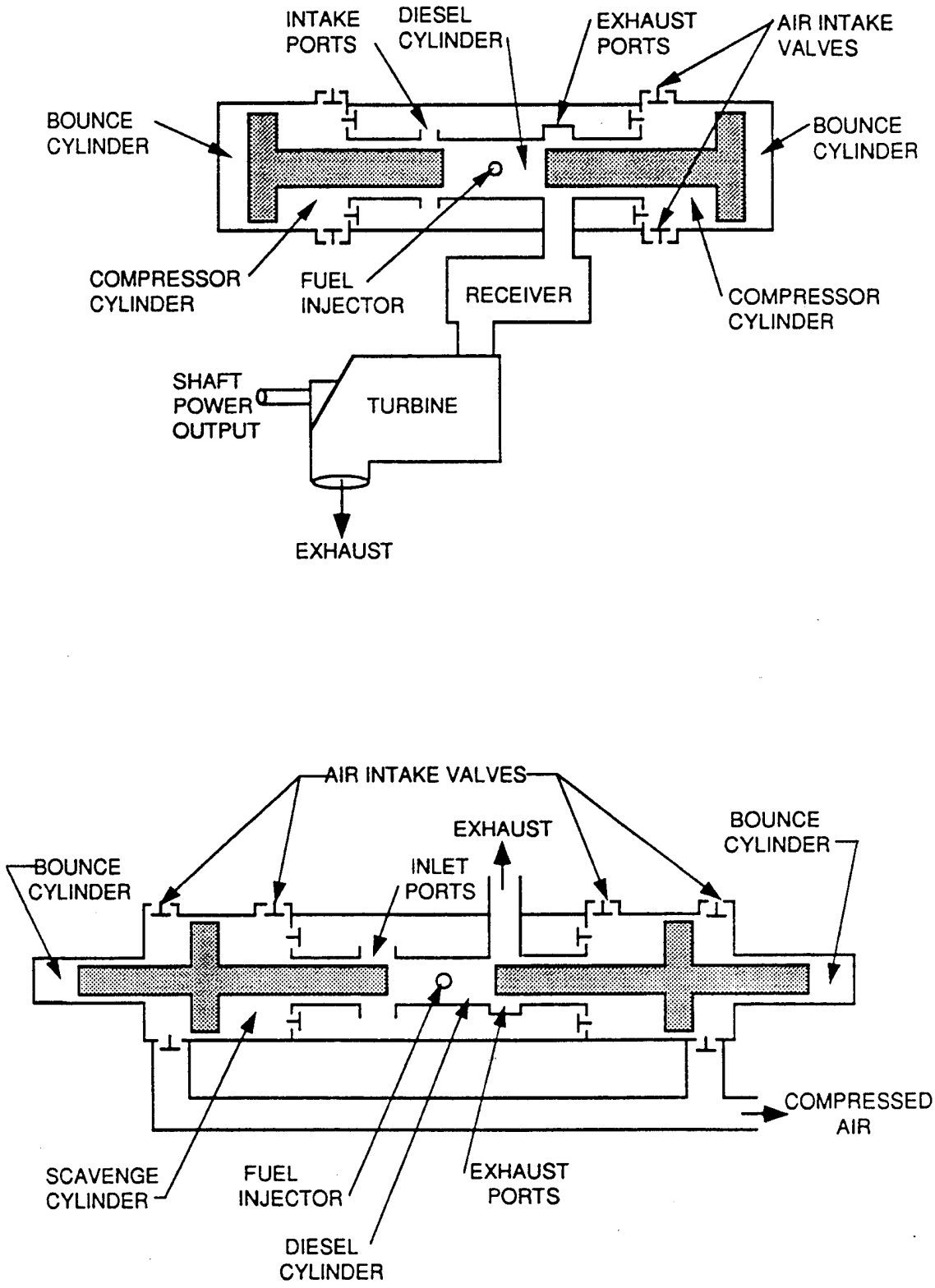

Figure 1. Typical free-piston engine, compressed air output

GENERAL CONFIGURATION -- DUEL ACTING FREE PISTON ENGINE - PUMP

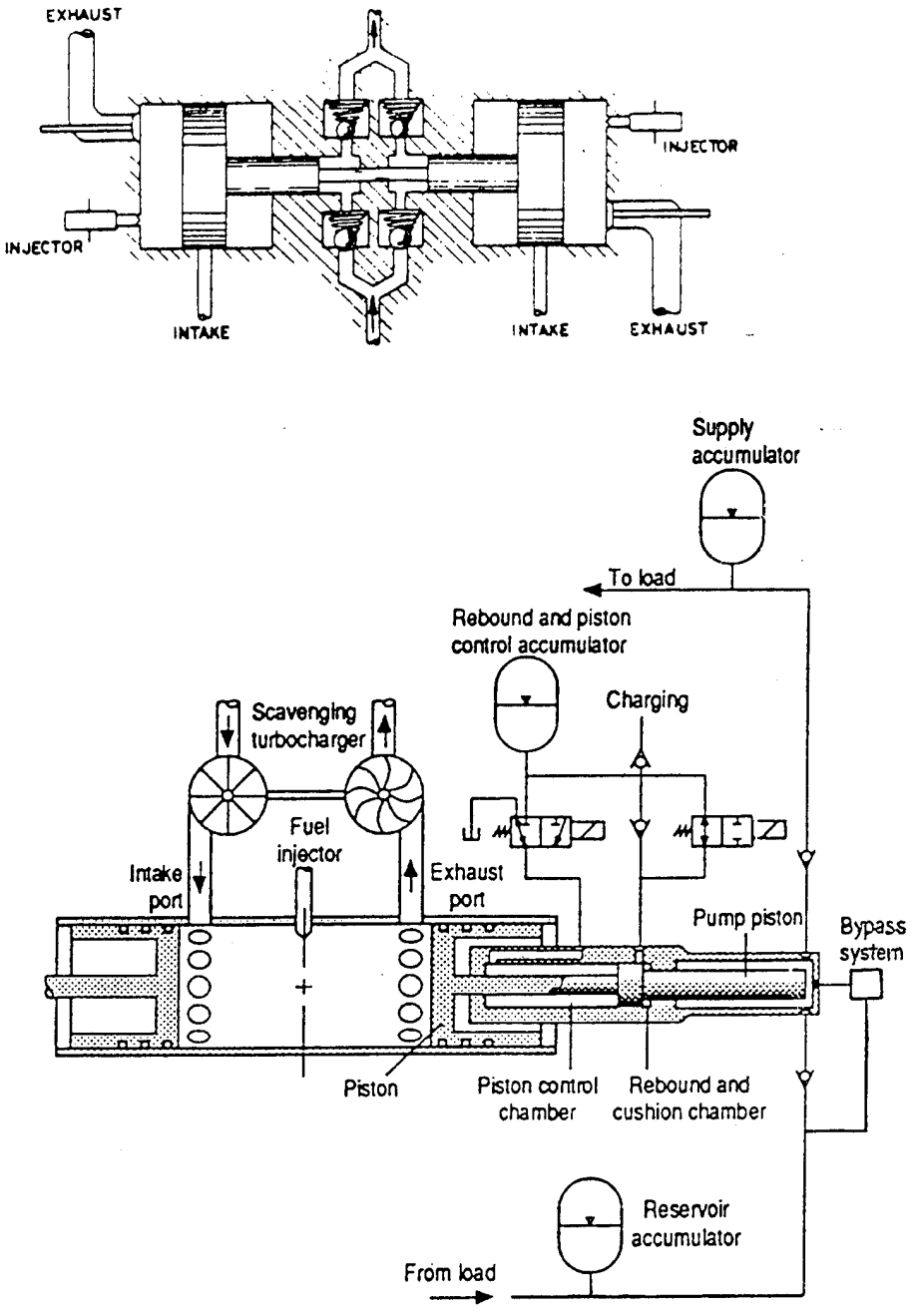

Figure 2. Free-piston engine – pump concept

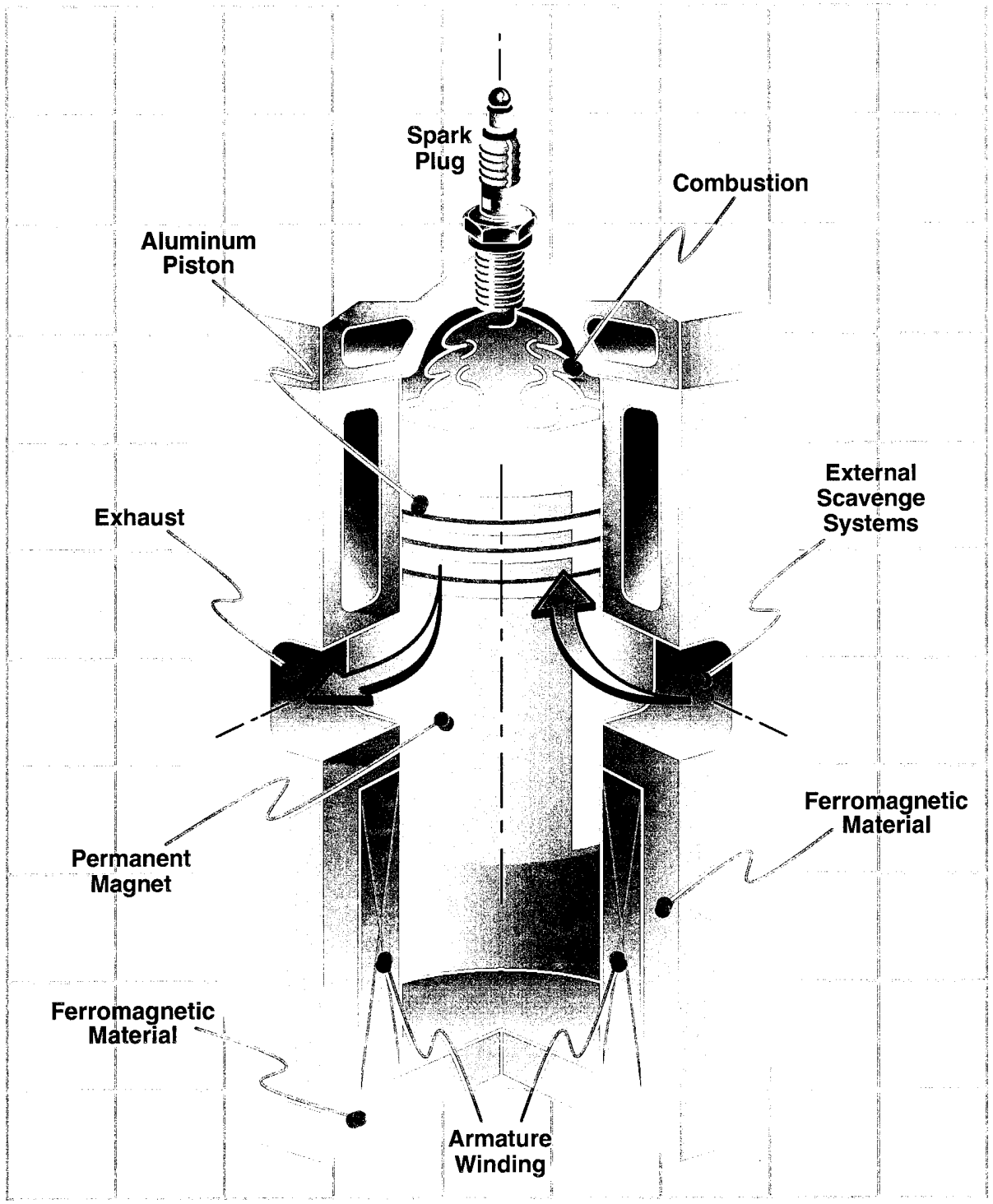

Figure 3. Free-piston engine – linear generator design

II. OBJECTIVE

The objective of this program was to evaluate the feasibility of a FPE coupled to a LG as an auxiliary power unit for a hybrid vehicle.

III. ENGINE MODEL

The engine that was modeled for this study was a single-cylinder, two-stroke, natural gas-burning engine. The engine was loaded with a linear generator that can be used to supply power to a HEV. The nature of the FPE concept is that piston motion characteristics are governed not by a mechanism but by the dynamic interaction of the engine and load. This requirement leads to some interesting design and control problems since the limits of piston motion, and hence compression ratio and displacement, are not fixed. Thus, the compression ratio and displacement are dependent upon the forces generated by compression and by the restoring force.

In order to properly match a load to the engine, it is essential to design the load such that its power absorption is matched to the power output of the engine, cycle-by-cycle. Otherwise, the piston unit will be in danger of striking either the cylinder head or the mechanical limit at the opposite end. A linear generator is well suited to this application, because its power absorption can be controlled by the excitation on a cycle-by-cycle basis.

To assist in the design process, Southwest Research Institute (SwRI) has prepared an engine simulation program that simulates the fundamental physical processes occurring in the engine and linear generator. The program requires a fairly extensive list of inputs describing the engine, the operating conditions, and the component characteristics (valve sizes and dynamics, ring pack design, etc.). As output, the program provides a comprehensive set of data including pressures, temperatures, and masses in each of the control volumes throughout the cycle, estimates of engine performance, and instantaneous flowrates through each of the valves and pipes.

This program was used in conjunction with the models developed for the linear generator to evaluate generator designs and control issues. This report briefly describes the mathematical models used, the engine, and the results from the simulation using the preliminary design parameters.

A. Modeling Approach

The engine simulation code adapted by SwRI for this project was designed to provide a complete thermodynamic simulation of the engine. The engine cylinder and scavenging chamber are treated as thermodynamic control volumes, with uniform pressure and temperature, and with varying volume. Quantities passing the control volume boundaries include heat, work, mass, and energy (carried by the mass). Manifolds and intercoolers are treated as fixed-volume control volumes; they are similar to the engine control volume with the exception that no work crosses their boundaries. Mass flow between volumes is handled by a set of subroutines that simulate the dynamic propagation of pressure waves through the pipes, using an implementation of the method of characteristics.

The piston motion is governed by integration of the second-order equation of Newtonian linear motion *(F=ma)*. The sum of forces includes the electromagnetic forces and the pressure forces on the engine piston (both cylinder and scavenge chamber), the bounce chamber, and friction forces calculated for the rings. The program thus updates piston position and velocity at each timestep, and provides a true transient simulation of the engine performance.

B. Engine Design Concept

The engine is shown schematically in Fig. 4. For the modeling study, the engine uses a single free piston to drive the linear generator. In the production or prototype design, an opposed piston arrangement would be used to obtain a balanced engine.

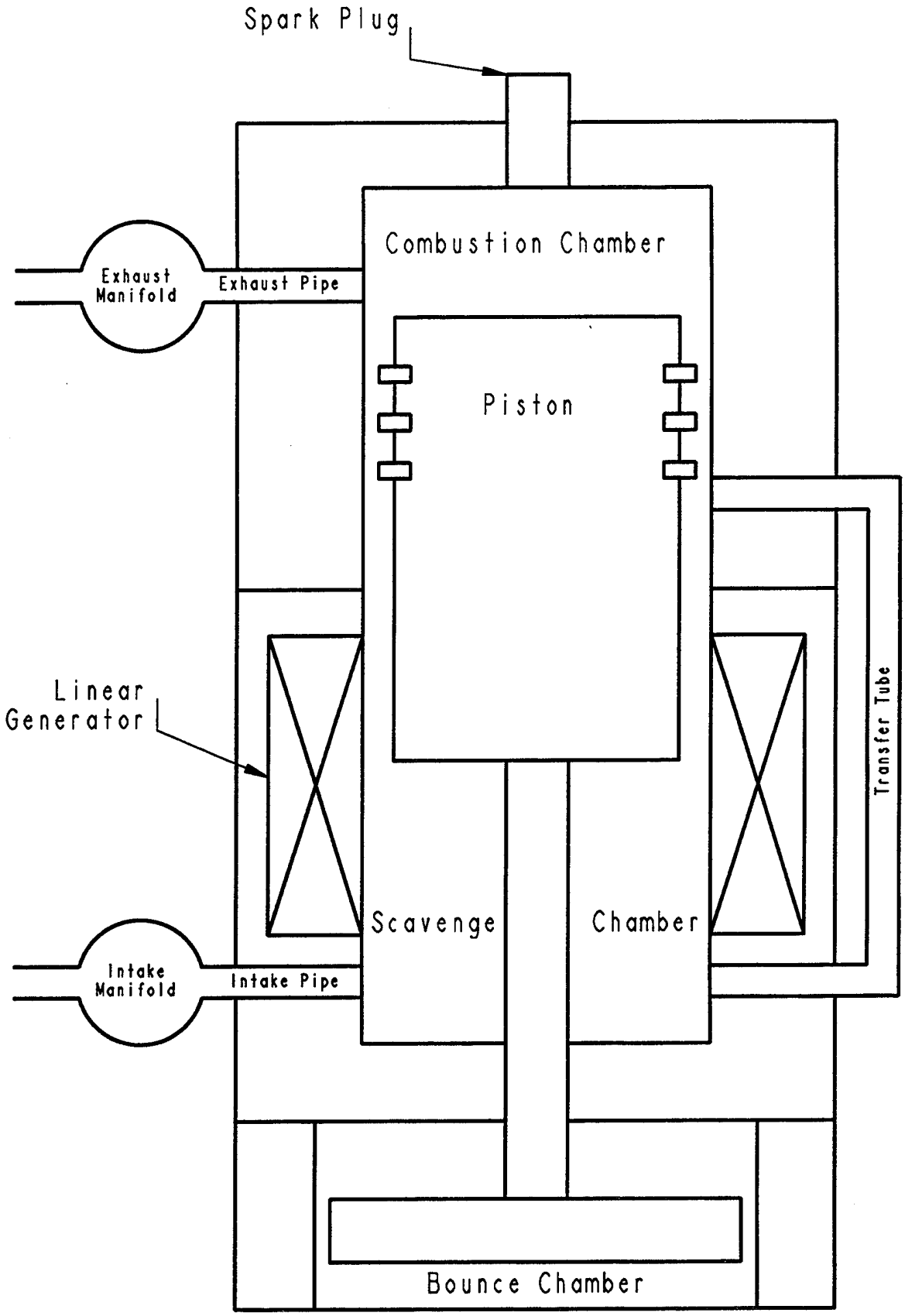

Figure 4. Free-piston engine – linear generator schematic

C. Physical Description

The engine receives ambient air through an inlet restriction into the inlet manifold. The air then feeds through a pipe segment, and a reed valve, to the scavenging chamber. The scavenging chamber is connected to the engine cylinder through a transfer tube. The exhaust port is connected to the exhaust manifold, through the exhaust pipe. The exhaust products exit the manifold to the ambient through a short pipe segment. The program provides the capability for an exhaust back pressure different from the inlet pressure.

D. Cycle Description

The engine is a two-stroke, loop-scavenged engine. At rest, the piston is at bottom dead center (BDC), the linear generator is de-energized, and the pressures throughout the engine are in equilibrium with the atmosphere. In order to start the engine simulation, an initial force was applied to the piston. This force simulates the force that would be imported to the piston if the LG were used in reverse to accelerate the piston to top dead center (TDC). As the piston travels toward TDC, two events occur. First, the piston travel creates a low pressure in the scavenge chamber, drawing in ambient air from the intake manifold. Second, the piston compresses the air in the combustion chamber and provides a force to return the piston to BDC when the linear generator is de-energized.

As the piston returns to BDC, it uncovers the exhaust port, blowing down the pressure in the combustion chamber. As piston travel continues the intake ports are uncovered. As the piston approaches BDC, it compresses air in the scavenge chamber. The compressed air is then forced into the combustion chamber as the intake port opens. The downward motion of the piston also compresses air in the bounce chamber, which provides the force for the return of the piston to TDC during engine operation.

During normal engine operation, the bounce chamber provides the force for returning the piston to TDC, compressing the fuel/air mixture in the combustion chamber prior to ignition. After

ignition, the piston will be accelerated downward. Energy will be absorbed from the piston by the linear generator and the bounce chamber.

IV. LINEAR GENERATOR PRINCIPLES

Five distinct linear generator concepts have been studied as part of this program. These concepts include the permanent magnet generator, the reluctance generator, the linear direct current (DC) generator, and the three-coil and two-coil induction generator concepts. The following paragraphs discuss each of these five concepts, outline the procedure utilized to study the concept, and highlight the concept's advantages and disadvantages.

A. The Permanent Magnet Generator

Figure 5 illustrates the permanent magnetic generator concept. As its name implies, this generator concept utilizes permanent magnets mounted on the piston to create a moving field of magnetic flux. When this moving field passes through the stationary armature winding, a voltage is induced and current flows into the load.

The permanent magnet concept has one extremely attractive attribute. Because permanent magnets require no external excitation, no mechanical or electrical connections to the moving piston are required. Furthermore, the stationary armature circuit is very simple, consisting of a wound coil and a full-wave rectifier bridge (to allow power delivery to the load regardless of the piston's direction of motion).

Unfortunately, a host of difficulties plague the permanent magnet concept. The most pronounced of these difficulties are the environmental limitations of contemporary magnetic materials. Permanent magnet materials have reduced performance and lifetime when exposed to high temperatures, high vibration levels, or both. The best magnetic materials available today are of the neodymium-iron-boron variety, but these materials are very difficult to use with temperatures over 100°C. For very high temperature applications, Alnico or rare-earth cobalt magnets must be used.

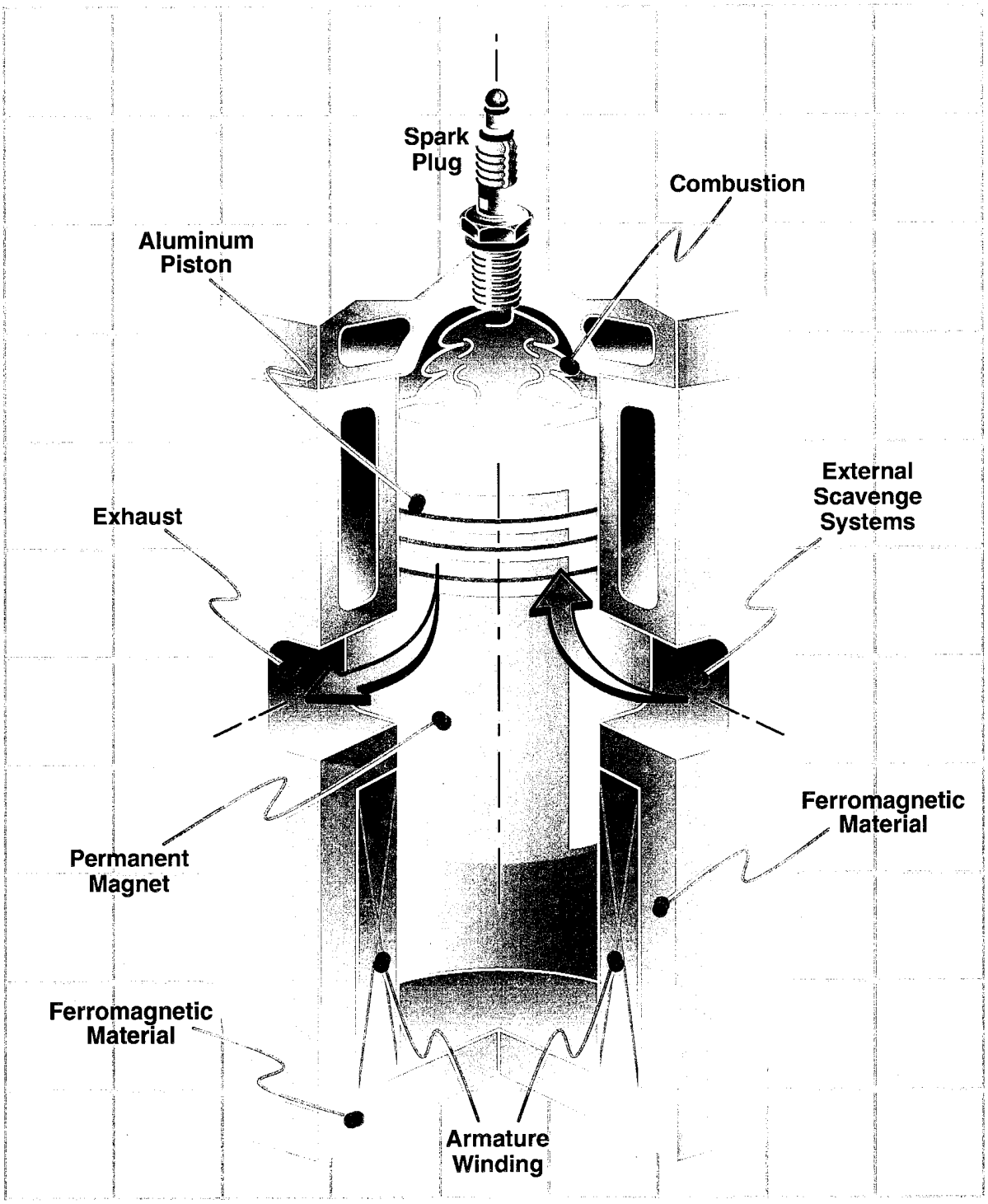

Figure 5. Permanent magnet generator schematic

The extreme temperatures present in and near the combustion chamber of internal combustion engines make utilization of permanent magnets an extremely risky proposition. The highly vibratory nature of the engine operation exacerbates this problem still further. Exposure to shock-type mechanical loading tends to reduce the magnetization of permanent magnets, and repetitive exposure to such effects could, over time, drastically reduce the performance of any available permanent magnet.

Finally, the weight of available permanent magnets represents an important issue in this application. The operational speed of the piston is critically dependent on piston weight, and the induced voltage is proportional to the speed. The addition of heavy permanent magnets to the piston will lower the piston's speed and adversely impact the voltage-producing capability of the system. The problems discussed above are related to the physical properties of contemporary magnetic materials, and may be overcome by future technological advances. However, other disadvantages of the permanent magnet concept are more fundamental. These disadvantages are related to the lack of controllability involved in the concept. The magnetic field produced by permanent magnets cannot be changed easily under electronic control; so thus the voltage produced by the generator will be fixed and unadjustable. This restriction is inconsistent with the project goals of controlling engine speed electronically and also does not allow operation of the generator as a motor to start the free piston engine. These unsurmountable problems led to early rejection of the permanent magnet concept, and no detailed theoretical or numerical analysis of such systems was performed.

B. The Reluctance Generator

Figure 6 illustrates the reluctance generator concept. Suitable specimens of ferromagnetic material are mounted to the piston; their motion changes the mutual inductance between the separate, stationary excitation, and armature coils. The instantaneous voltage induced in the armature coil is equal to the product of the excitation coil current and the time rate of change of the mutual inductance between the coils. This concept shares the primary advantage of the permanent magnet approach i.e., no mechanical or electrical connections to the piston. The

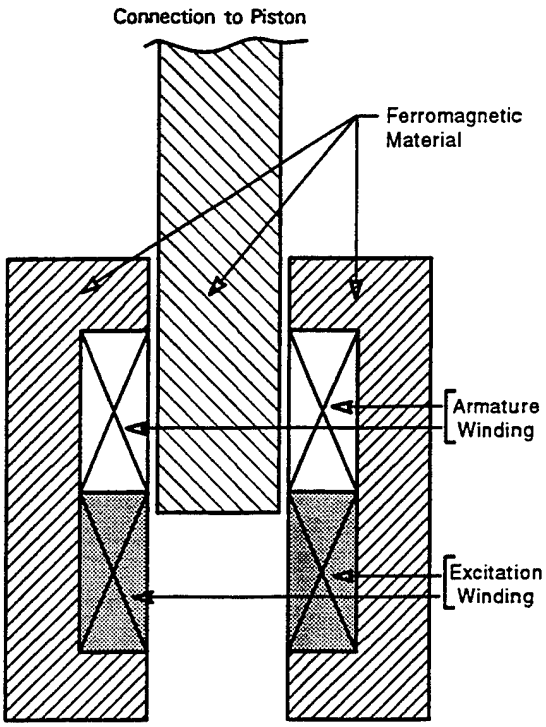

Figure 6. Reluctance generator schematic

reluctance generator concept overcomes the difficulties associated with operating permanent magnets under such adverse conditions and offers controllability by adjusting the excitation current. However, ferromagnetic materials are relatively heavy, so the piston weight problems encountered in the permanent magnet concept apply to the reluctance concept as well. Because investigators believed that the performance of the reluctance approach could be rivaled or surpassed by concepts utilizing lightweight aluminum pistons, the reluctance concept was not pursued in detail.

C. The Linear DC Generator

Figure 7 illustrates the linear DC generator approach. A stationary ferromagnetic yoke is used to guide flux and reduce excitation requirements while a stationary excitation coil produces an air gap flux field. The armature coil is mounted on the piston and moves in the air gap field. The voltage induced in the armature is applied via sliding brush contacts to the load.

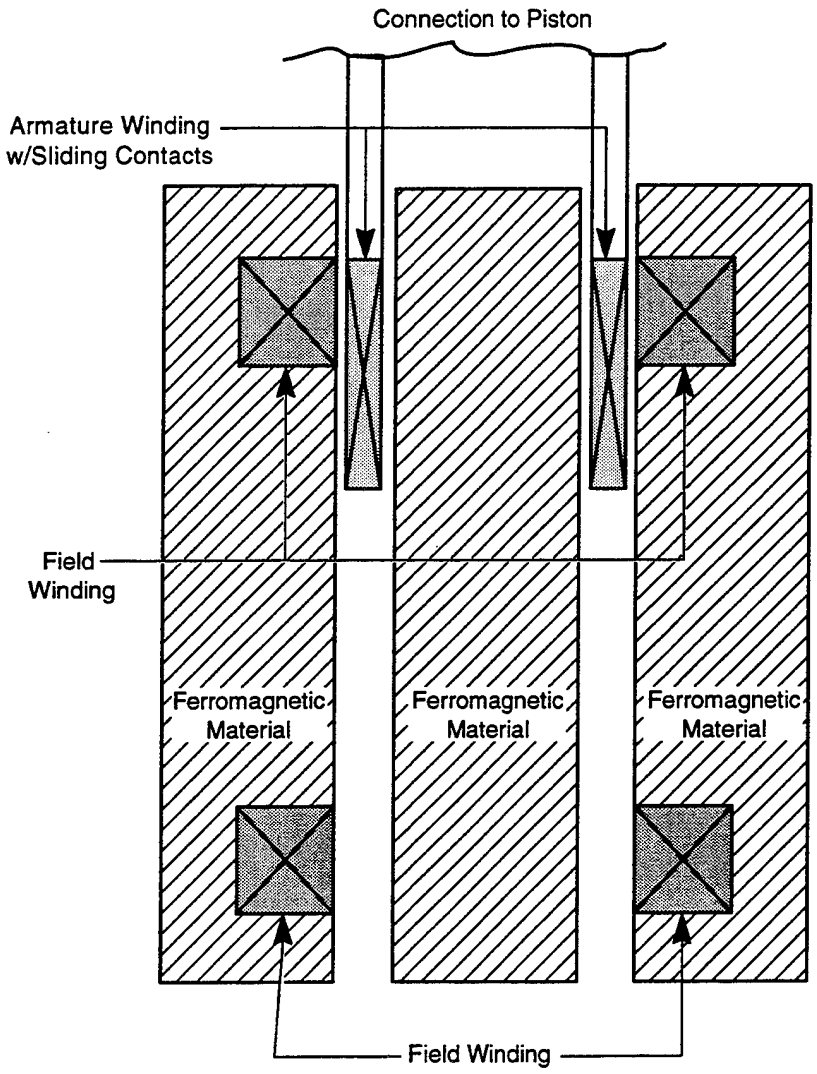

Figure 7. Linear DC generator

This approach has the advantage of extreme conceptual simplicity. This approach is the first that was analyzed in detail and the first that showed the potential for operation at high efficiency (90 percent range). The primary disadvantage of this concept is the need for sliding electrical contact between the piston and the stationary components of the system. However, these are low-current (100 A), low-velocity (20 m/s) sliding contacts; the investigator have developed and successfully operated far more ambitious sliding contacts in the past. Because this concept represented a relatively low-risk route to a successful system, a detailed "pencil-and-paper" analysis was conducted, and the resulting design was treated as a fallback position while more ambitious and sophisticated concepts were pursued.

The analysis of the linear DC generator is quite straightforward. Figure 8 illustrates the flux paths in the machine, as well as the pertinent physical dimensions. The saturation flux density (B_{sat}) of typical ferromagnetic materials is around 1.8 Tesla (T). The total flux crossing the air gap must equal the total flux leaving the ends of the central ferromagnetic cylinder since the area of the cylinder ends is less than that of the surface facing the air gap, it is the flux density through the cylinder ends that is limited to B_{sat}. The air gap flux B_{gap} is computed via the following formula:

$$2\pi r l B_{gap} = 2\pi r^2 B_{sat} \qquad \text{(Eq. 1)}$$

$$B_{gap} = \frac{r}{l} B_{sat} \qquad \text{(Eq. 2)}$$

where:

r = armature of radius

l = distance between coils

B_{gap} = magnetic flux density in the air gap

B_{sat} = saturation magnetic flux density.

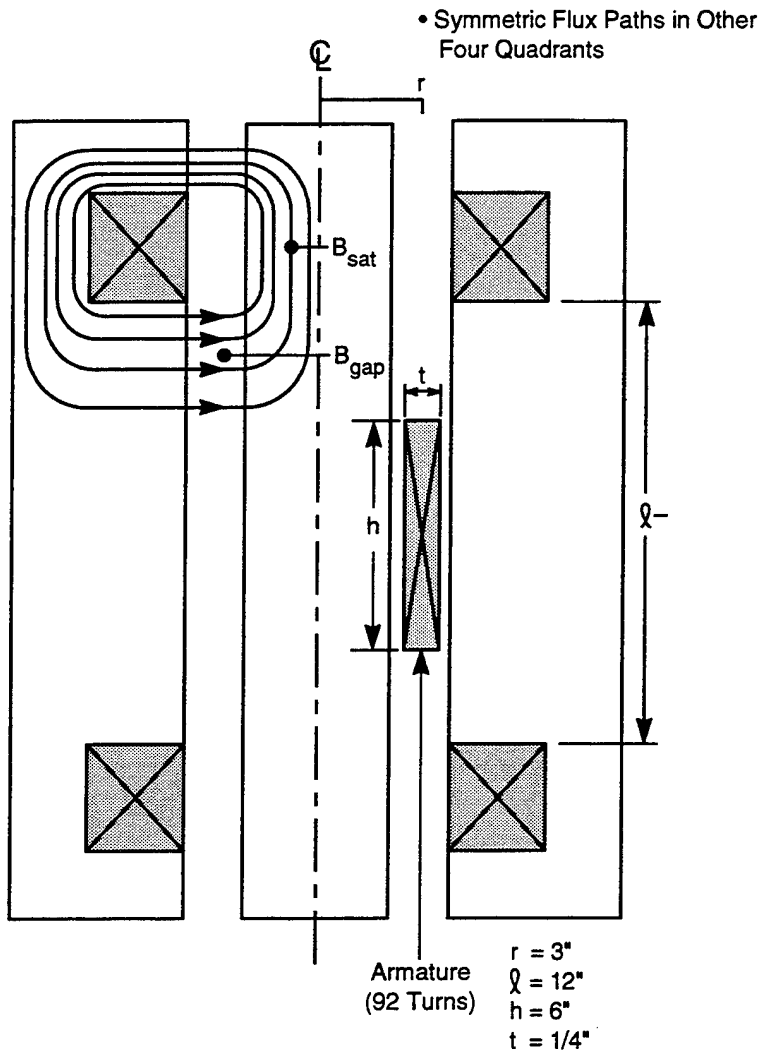

Figure 8. Flux paths plus dimensions in the linear DC generator

Substitution of the appropriate dimensions indicates that the air gap flux must be limited to 0.45 to 0.5 T in order to prevent saturation in the areas of peak magnetic flux density. The induced armature voltage is equal to the product of the air gap flux, the length of the armature coil, and the piston velocity. Numerical investigations performed with the free-piston engine code indicated an average piston velocity of approximately 12 m/s. Assuming an air gap flux density of 0.5 T and a required output voltage of 265 V, the required armature winding length is 44.1 meters. This length is equal to the product of the armature coil circumference and the number of armature turns; the resulting required turn count is 92. The turn count and the armature dimensions specified in Fig. 8 allow straightforward computation of the armature resistance:

$$R = \frac{2\pi r}{\sigma p t l} \qquad \text{(Eq. 3)}$$

where:

r = armature of radius

t = armature thickness

l = armature length

p = packing factor

σ = conductivity of armature material.

For aluminum wire and a 50-percent packing factor, the resistance is approximately 250 μΩ. For a constant armature current of 100 A, the associated resistive losses are approximately 2.5 kW, or about 10 percent of the total mechanical power produced. Of course, further losses occur in the battery resistance, and losses are increased still further if the armature current maintains an average value of 100 A but deviates from a totally constant wave form. However, a careful design might surpass the 50-percent wire packing factor. Because the armature sleeve is so thin (0.25 inch), utilization of copper rather than aluminum would have little adverse impact on the total piston mass.

In addition, losses occur in the field winding. Because this winding is stationary, however, it can be whatever size is necessary (within reason) to reduce the resistive losses to a negligible level. For the system shown in Fig. 8, the total field winding losses are well under 500 W.

The linear DC concept was developed far enough to be certain of its viability. However, because this concept requires sliding electrical contacts, the analysis was terminated at this point. Work on more sophisticated concepts was initiated.

D. The Three-Coil Induction Generator

Figure 9 illustrates the three-coil induction generator concept. In essence, the monolithic conductive sleeve attached to the piston functions as a "shutter" that controls the amount of flux produced by the field winding that cuts the armature winding. The time variation of this flux induces the required voltage in the armature. Once again, the (stationary) ferromagnetic materials in the system guide flux and reduce the excitation requirements.

Each of the three coils has self inductance and mutual inductance with the other two coils. The mutual inductance matrix associated with this system can be written as in Equation 4:

$$L = \begin{bmatrix} L_f & M_{fa} & M_{fp} \\ M_{fa} & L_a & M_{ap} \\ M_{fp} & M_{ap} & L_p \end{bmatrix} \qquad \text{(Eq. 4)}$$

where:

L = inductance

M = mutual inductance between z coils indicated by subscripts

a = armature coil

p = piston

f = excitation coil.

A flux conservation approach can be used to analyze this concept. Because the system contains three independent coils, the algebraic manipulations involved are quite complex. Investigators utilized Maple, a symbolic mathematics package available to carry out the necessary manipulations.

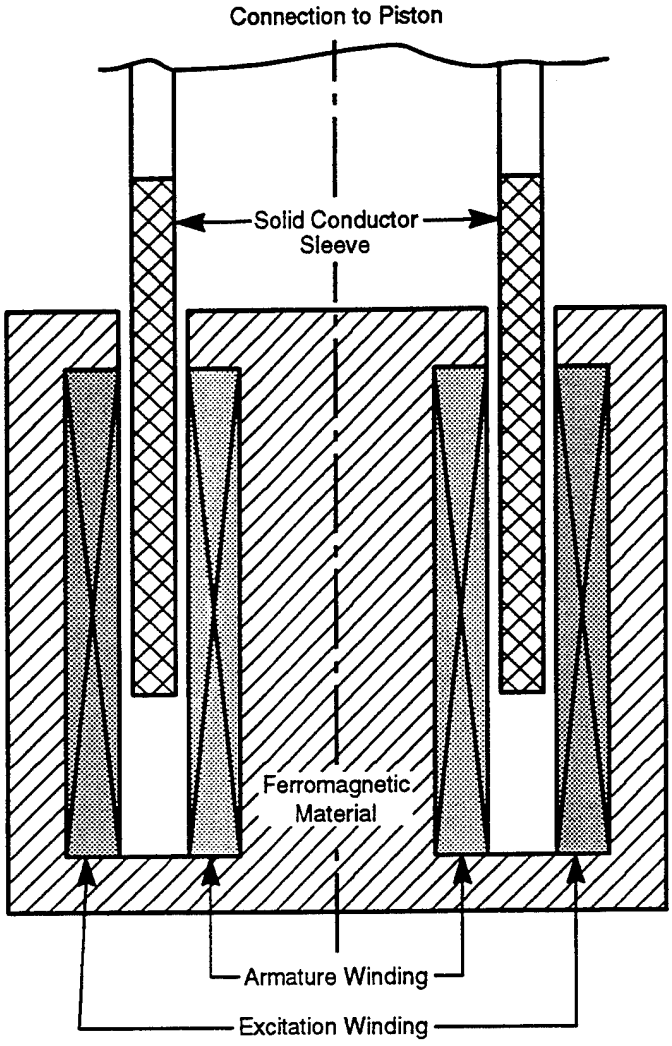

Figure 9. Three-coil induction generator schematic

Since the field-to-piston and armature-to-piston mutual inductances vary, the entire inductance matrix can be regarded as a function of piston position. However, if losses are neglected, the flux linkages established in each of the three coils will remain unchanged as the piston moves; the coil currents will adjust themselves to whatever values are necessary to maintain constant flux linkages in all coils. Thus

$$I(x) = L^{-1}(x)\ \lambda \qquad \text{(Eq. 5)}$$

where $I(x)$ denotes the vector of position-dependent currents λ denotes the vector of constant flux linkages. The magnetic energy stored in the system is given by the expression

$$E(x) = \frac{1}{2}\ \lambda^t\ L^{-1}\ (x)\ \lambda \qquad \text{(Eq. 6)}$$

The fundamental analysis technique pursued involved the following steps:

1. Select a trial value for the flux linkage vector.

2. Compute the magnetic energy stored in the system with the piston fully "out."

3. Compute the magnetic energy stored with the piston fully "in."

4. The mechanical power converted to electrical form is the difference between the quantities computed in steps 3 and 2.

5. Evaluate approximate losses by computing the current values at each position of the piston. Large fluctuations in coils current can create efficiency problems.

Utilizing finite element analysis techniques, investigators computed the matrix L at a variety of positions and fit polynomial functions to the results. This procedure allowed rapid and accurate approximation of L and its inverse at any piston position. The analysis procedure outlined above was performed. The last few lines of the output listing convey the most interesting information. The variable "ratio" has a value of approximately 65.7; this ratio indicates that the stored magnetic energy rises by this factor as the piston moves from the fully withdrawn position to the

fully inserted position. The free piston engine supplies the necessary energy by moving the piston through an opposing electromagnetic force.

The system operating frequency is approximately 50 Hz, and the required operating power is 25 kW. These values imply that, during each cycle, 500 J of energy should be converted, and that the necessary excitation energy (EnergyIn in the Maple analysis) should be 7.6 J. The unit excitation current utilized in the Maple analysis produced an excitation energy of 5.67×10^{-5} J, and EnergyIn is proportional to the square of the excitation current. The required excitation current, therefore, is 366.11 A.

Application of this value as a scale factor to the inserted position current vector IIn yields the actual values of the three coil currents at the inserted position; the stator current is 15.6 kA, the armature current is 11.2 kA, and the piston current is -26.7 kA. These values highlight the fundamental problem of the three-coil induction concept: even under idealized operation (no load resistance) the piston current takes on larger values than either of the other currents, and the ratio of the piston current to the armature (load) current becomes even larger when a practical load resistance is included in the armature circuit. Resistive losses in the piston far exceed usable energy delivered to the load; this phenomenon renders this concept useless for practical applications.

E. The Two-Coil Induction Generator

Figure 10 illustrates the two-coil induction generator concept. In this concept, the conductive sleeve attached to the piston acts as a shutter, controlling the area of the flux path through the air gap. This action causes the effective stator terminal inductance to vary with piston position and allows the system to generate a voltage.

The one coil accessible externally must provide both excitation and deliver generated power to the load. The external circuitry shown in Fig. 6 allows the coil to fill this dual role. The active current source produces the excitation current; the coil current never falls below this value. The

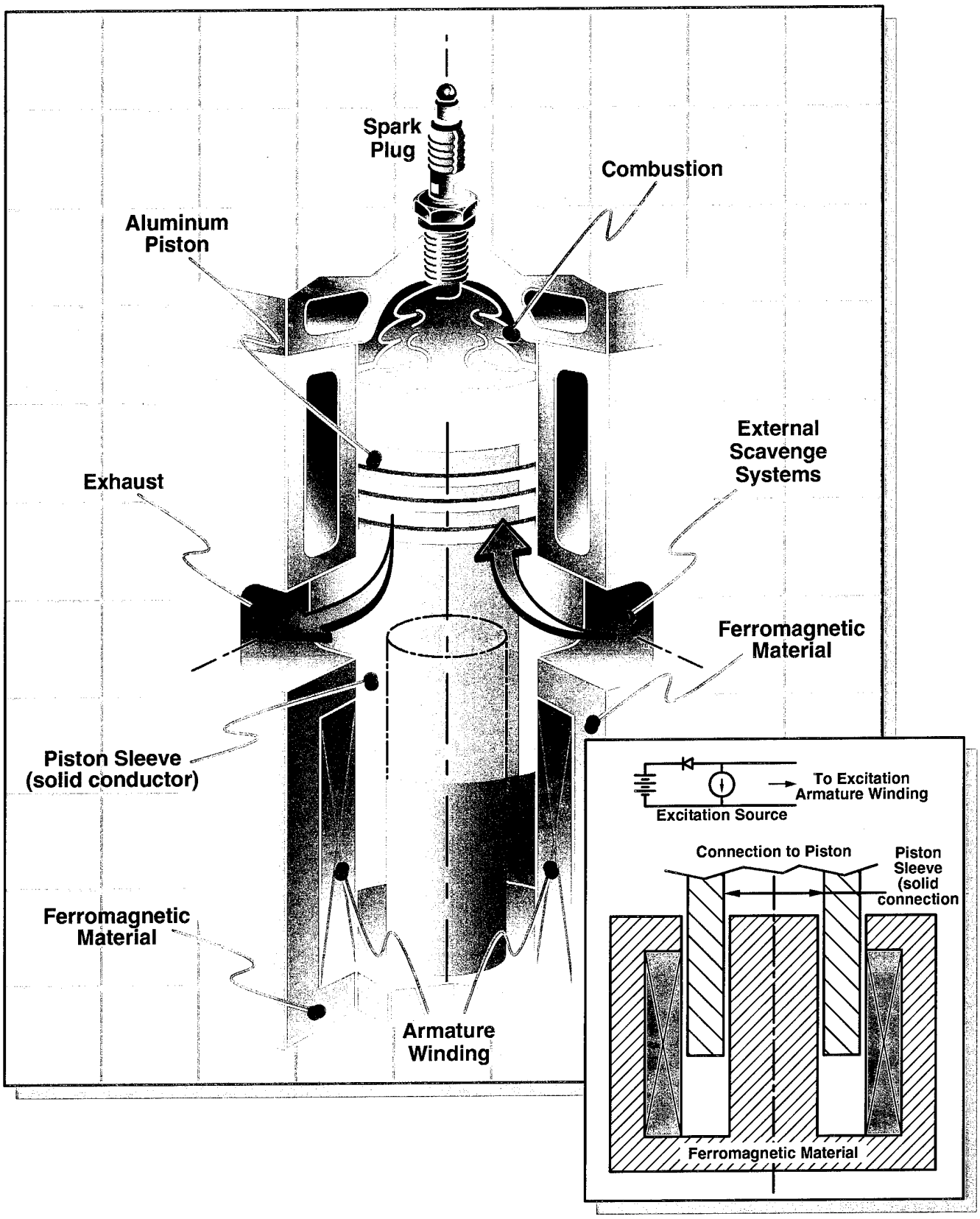

Figure 10. Two-coil induction generator

diode keeps the battery from producing an opposing current flow when the generated voltage is less than the battery voltage. During those portions of the cycle when the generated voltage rises above the battery voltage, however, the diode allows current and power to flow into the battery.

Preliminary evaluation of this concept indicated that it could produce the necessary power, but the concept was inefficient because the current pulses delivered to the battery were quite transient. The battery-charging power is equal to the product of the battery current and the battery voltage; total energy delivered to the battery is hence given by the time integral of this product. Since the battery voltage is constant, the energy delivered to the battery during any given time integral is proportional to the time integral of the current. Losses, however, are proportional to the time integral of the current *squared.* When the peak-to-average ratio of the current wave form rises, the current squared integral rises faster than the current integral, and efficiency suffers.

Investigators recognized that, in order to obtain maximum efficiency, it would be necessary to maintain a current wave form that was as constant as possible during the power stroke portion of the cycle. A straightforward technique to accomplish this end by varying the air gap width was developed. While precise implementation of this approach will involve considerable optimization based on finite element analyses, the technique can be derived in an idealized way quite simply, as shown below.

The pertinent "diode on" circuit equation for the system in Fig. 10 is:

$$L_c \frac{dI_c}{dt} + \left(v \frac{dL_c}{dx} + R_c + R_b \right) I_c = V_b - R_b I_f \qquad \text{(Eq. 7)}$$

where:

L_c = circuit inductance

I_c = circuit current

R_c = circuit resistance

R_b = battery resistance

V_b = battery voltage

I_f = excitation current

v = piston velocity.

If the algorithm successfully holds the battery-charging current constant, then its time derivative can be dropped from this equation. The remaining terms can be rearranged to solve for the inductance gradient:

$$\frac{dL_c}{dx} = \frac{1}{v}\left[\frac{V_b - R_b I_f}{I_c} - (R_c + R_b)\right] \qquad \text{(Eq. 8)}$$

All of the terms inside the brackets are constant, and those involving resistances are typically negligible (<10 percent) compared to the battery voltage term.

The inductance of the magnetic circuit configuration illustrated in Fig. 10 is given by the following equation:

$$L(x) = N^2 \int_0^x \frac{2\pi r \mu_0}{g(x)}\, dx \qquad \text{(Eq. 9)}$$

Differentiation with respect to position simply eliminates the integration, and the remaining equation can be solved for an explicit expression for the gap width:

$$g(x) = N^2 \frac{2\pi r \mu_0}{L'(x)} \qquad \text{(Eq. 10)}$$

Investigators utilized this idealized procedure to design a two-coil induction generator for the target parameters of this project. The resulting required and actual inductance vs. position profiles are shown in Fig. 11. The match is quite good, and deviates most strongly at the extreme ends of the stroke. This deviation results from magnetic fringing in those areas. Figures 12 through 14 illustrate some finite element flux plots for the system with the piston at various positions; the fringing at the ends of the gap is evident. It is anticipated that iterative refinement

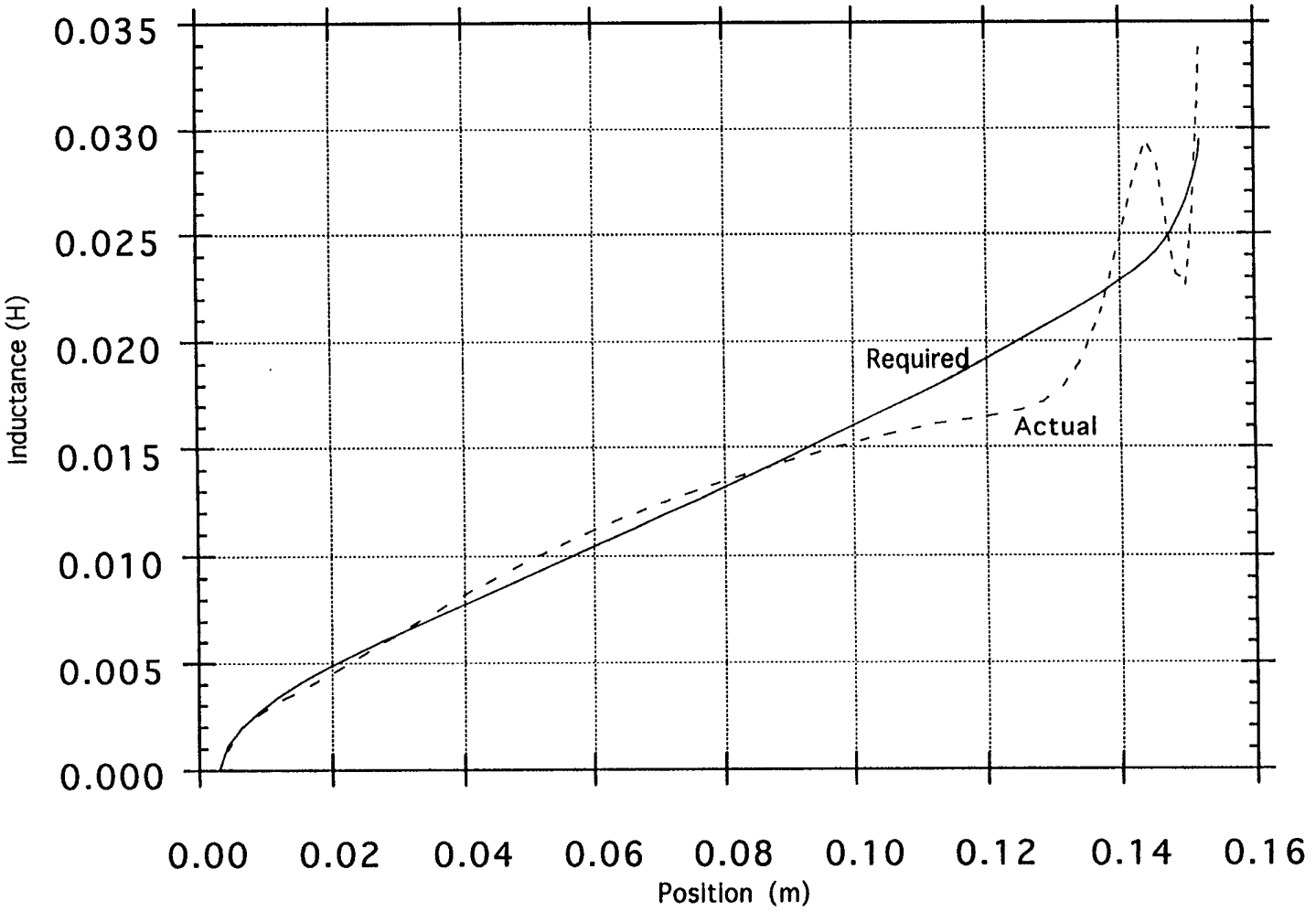

Figure 11. Actual versus required inductance profiles

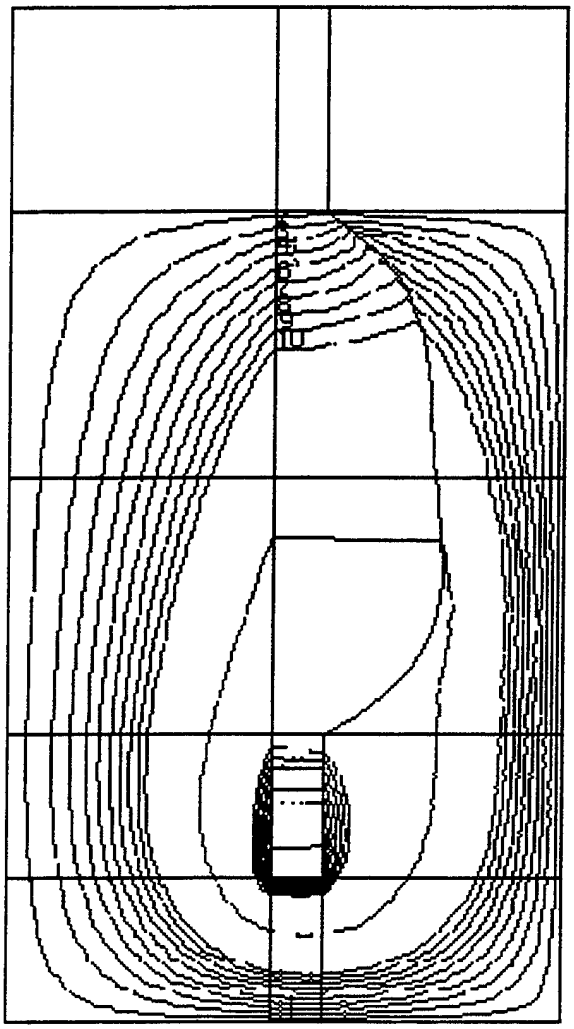

Figure 12. Plot of flux lines for two-coil induction generator with piston fully removed

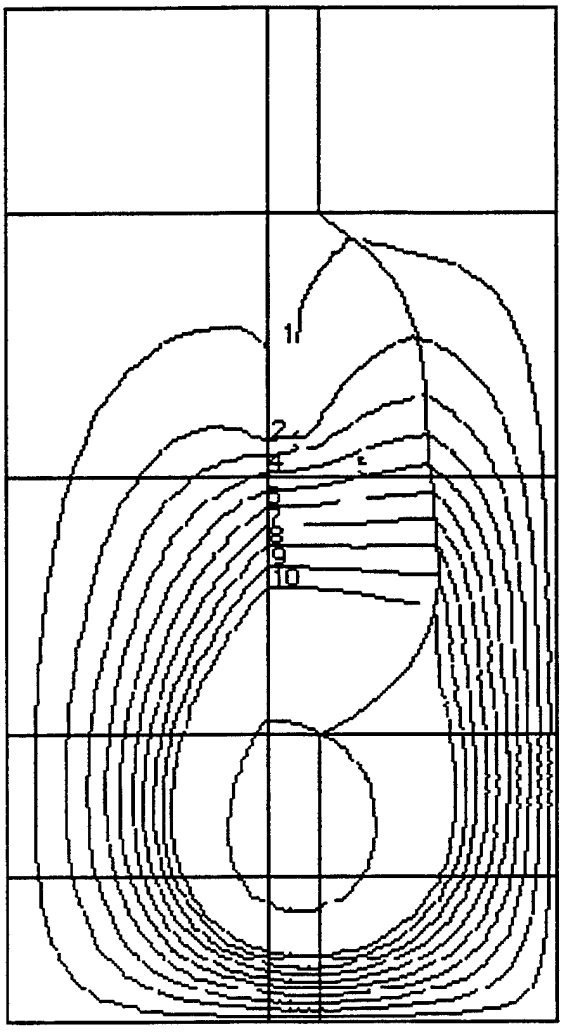

Figure 13. Plot of flux lines for two-coil induction generator with piston inserted half way

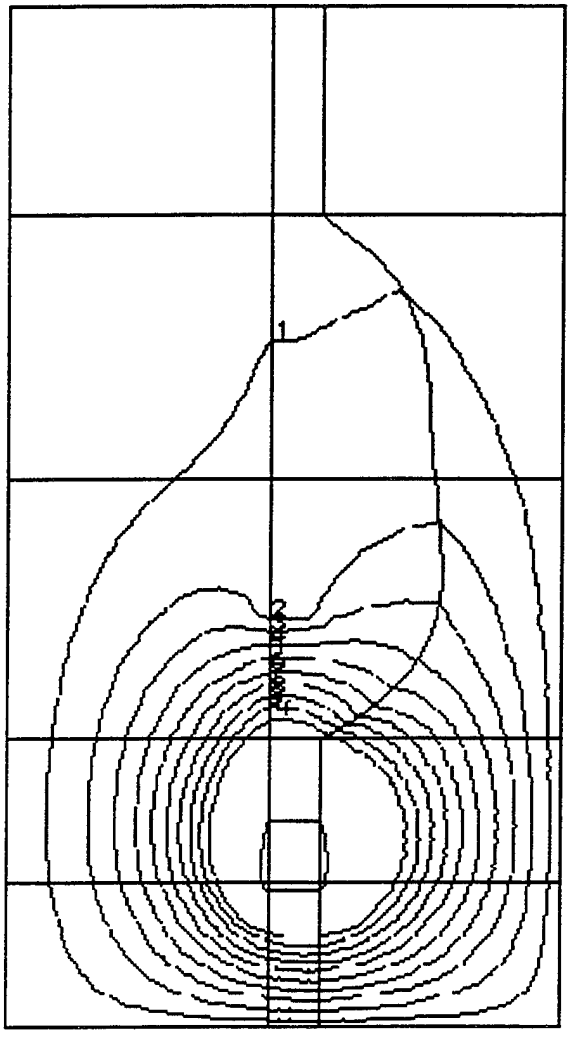

Figure 14. Plot of flux lines for two-coil induction generator with piston inserted all the way

of the gap shape will allow further improvement in the match between the actual and required inductance profiles.

V. MODEL RESULTS

This section presents various numerical results produced by an integrated free piston engine/linear generator point design based on the two-coil induction generator concept. The system simulated had a six-inch bore diameter, six-inch stroke, and a conducting sleeve 0.5 inches thick.

The system was designed to operate at approximately 25 kW mechanical power. Figure 15 illustrates the position dependence of various performance quantities associated with the operation of the system. The piston position is relative to the TDC mechanical limit. Because the system ultimately reaches a steady-state operating mode, all of these quantities are single-valued functions of piston position.

As illustrated in Fig. 15, the piston speed is approximately constant over a majority of the stoke. The linear generator was designed to provide a nearly constant flux density over the length of the stroke. However, at the end of the stroke the flux density increases by dramatically. The voltage generated is a product of the velocity and the flux density. When the velocity is low at the end of the stroke, the flux density is high. Hence, a nearly constant voltage is produced throughout the stoke of the engine.

The current is the difference between the generator voltage and the battery voltage, assumed to be 250 V, divided by the resistance of the generator. For this analysis, it was assumed that the internal resistance of the battery was negligible, essentially an ideal case. A rectifier circuit allowed current to only flow during the power stroke of the engine. The desired current profile is a square wave. The current profile that was obtained is somewhat less than ideal, but is actually quite good for this type of generator. As shown, the force acting on the piston is proportional to the current.

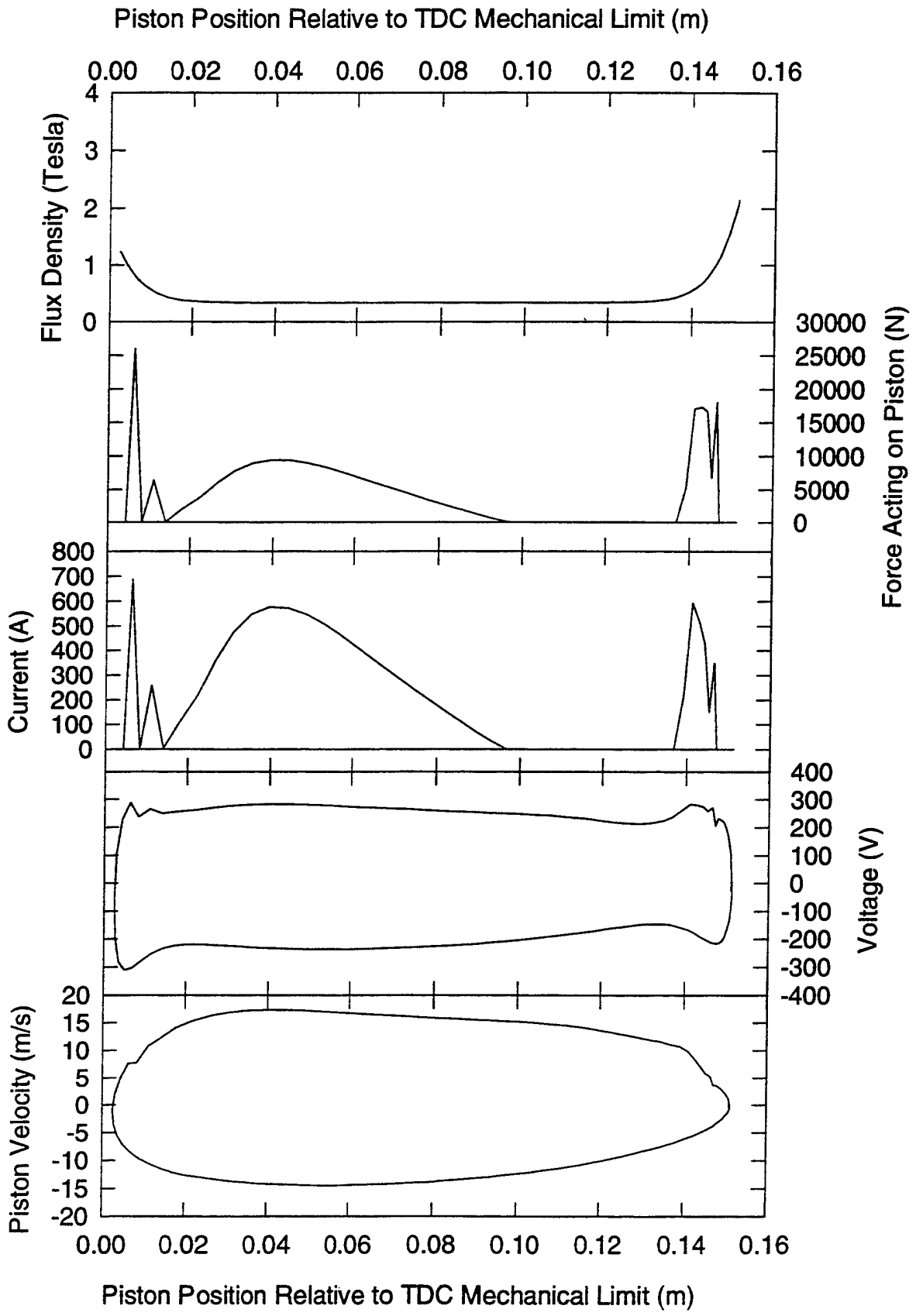

Figure 15. Linear generator parameters versus piston position

The power output of the system is established by two parameters: the manifold air pressure (increasing this pressure beyond one atmosphere is equivalent to turbocharging the engine, decreasing this pressure below atmospheric would represent throttled operation), and the intensity of the magnetic field in the air gap. Parametric studies were conducted varying each of these parameters. In order to evaluate the generator without taking into account the charging efficiency of the battery, the battery internal resistance was assumed to be zero.

The efficiency of the linear generator at the design point of 25 kW is approximately 90 percent with an estimated brake thermal efficiency of 27 percent. Figure 16 illustrates the impact on efficiency of varying the power output by changing the manifold air pressure. The generator power decreases as the indicated engine power increases. This phenomenon is a result of higher internal losses due to higher currents at the higher power. The engine compression ratio and the brake thermal efficiency, are for the most part, independent of indicated power. Variations in the brake thermal efficiency are primarily a function of the combustion model and not the linear generator.

The indicated power or the power produced by combustion is controlled mainly by the amount of fuel in the combustion chamber. The electrical power is obviously also dependent on the energy released during the combustion event, but it is also dependent on the excitation voltage to the linear generator. The excitation voltage determines the load on the generator. A higher loading produces a higher flux density and extracts more energy from the piston. At a fixed fuel rate, there is only a fixed amount of energy to extract. Therefore, a higher EM load tends to shorten the time over which the energy is extracted. A shorter stroke and lower compression ratio result. Figure 17 illustrates the effect of magnetic field strength on generator performance. The figure indicates that the engine speed and compression ratio can be varied over a relatively wide range by adjusting the EM loading. Consequently, EM load variation can be used for a variety of control purposes such as synchronizing multiple pistons, adjusting for fuel compositions, or changing engine speed.

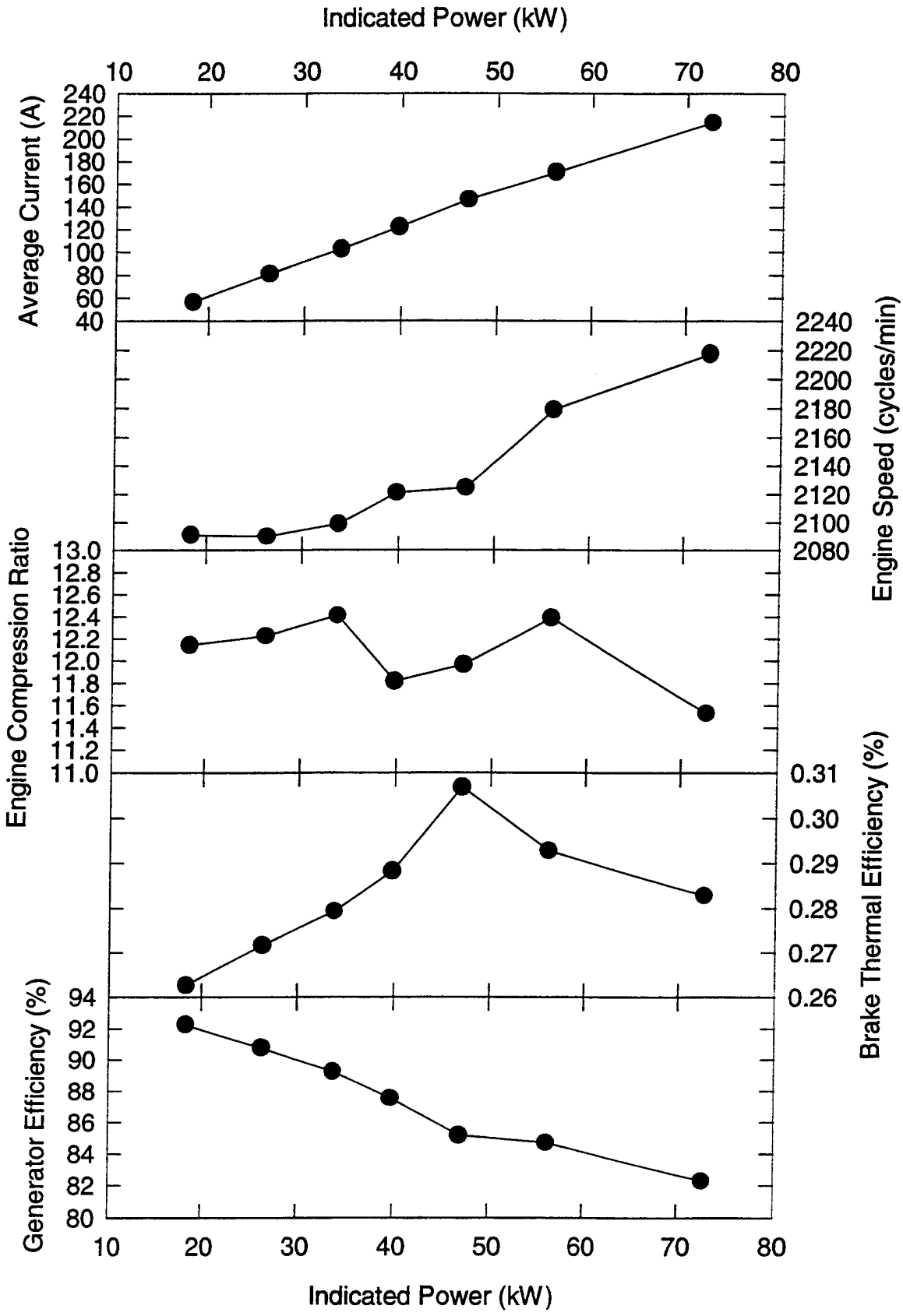

Figure 16. Performance parameters versus engine indicated power

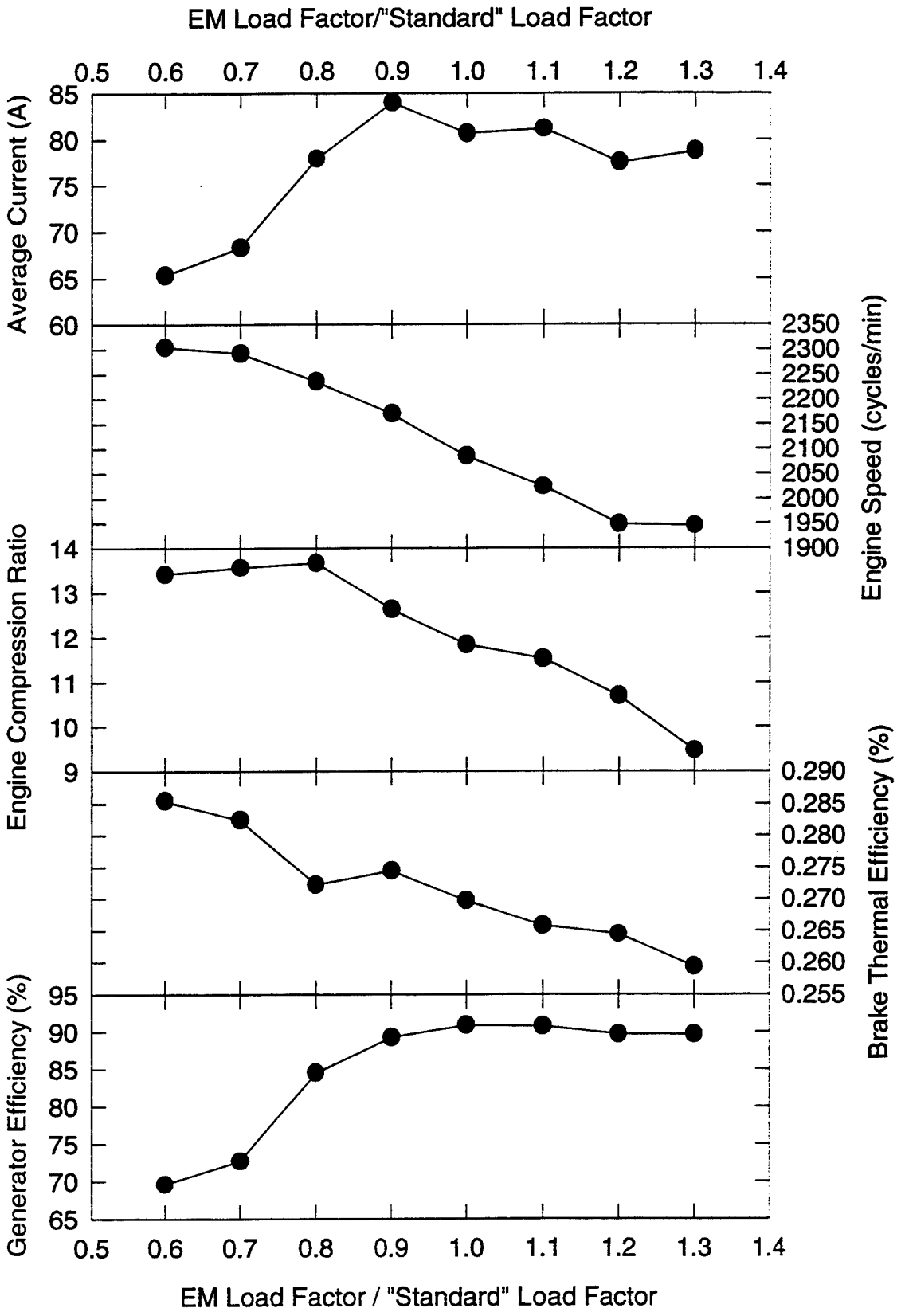

Figure 17. Performance parameters versus EM load factor

VI. SYSTEM IMPLICATIONS - SCALING

Analysis of the effect of general changes in generator geometry is quite difficult, requiring application of finite element techniques. However, the effect of changes in the system scale (i.e., so called "xerox" scaling) can be studied in a straightforward manner. In particular, the scale dependence of such critical variables as power and efficiency can be determined quite readily.

The scaling analysis begins with the determination of the scale dependence of the inductances and resistances of the generator. It is assumed that all pressures and magnetic field levels are unchanged as a consequence of the scale change (for very small scales, the system may be current density limited rather than magnetic field density limited). Stored magnetic energy is related to inductance by the expression

$$E = \frac{LI^2}{2} \qquad \text{(Eq. 11)}$$

Volumetric energy density is proportional to the magnetic field intensity squared. Thus, for unchanged magnetic fields, the stored energy is proportional to the volume, or to the cube of the system scale. The quantity LI^2 must also vary as the cube of scale.

The scale dependence of the current follows from Ampere's Law:

$$\oint Hdl = NI \qquad \text{(Eq. 12)}$$

Since the length of the path of integration varies with the first power of scale, and the point-by-point value of H should remain unchanged (scale-independent magnetic field density assumption), the value of I must vary as the first power of scale as well.

Since E varies as the cube of scale while I varies as the first power of scale, the inductance must also vary as the first power of scale. Determination of the scale variation of resistance is straightforward. The general expression for resistance in terms of geometric quantities and material properties is

$$R = \frac{l}{\sigma A} \qquad \text{(Eq. 13)}$$

where l is the length of the conducting path and A is its cross-sectional area. Clearly, the resistance is inversely dependent on the first power of scale.

Given these results for the scale dependence of inductance and resistance, the scale dependence of the L/R time constant follows directly. The time constant represents the time period over which the system loses a certain portion of the stored energy through resistive dissipation, and is proportional to the square of the scale.

The scale dependence of the time constant is the fundamental result required on the electrical side of the system. The next step in the overall scaling analysis is the determination of the effect of scaling on the engine's speed of operation and on the quantity of energy converted each period.

Free-piston engine speed is relatively independent of load and is governed by the mass of the piston and the stiffness of the spring-like components of the system (e.g., compressed air rebound). The frequency (ω) of a spring-mass system is given by the expression

$$\omega = \sqrt{\frac{k}{m}} \qquad \text{(Eq. 14)}$$

where k is the spring constant and m is the piston mass. The piston mass clearly varies as the cube of scale, since it is the product of a volume and a scale-independent density. The spring constant has the dimensions of force divided by length, or N/m, and represents the rate at which the spring force changes as its deflection is altered. In the free piston generator the force is produced by gas pressure acting on the piston face. If the gas pressure is treated as a scale-independent quantity, then the force varies as the piston surface area, or as scale squared. The distance required to produce equivalent deflection varies as the first power of scale. The spring constant, therefore, varies as the first power of scale. This ratio indicates that the resonant

frequency varies as the inverse first power of scale; the stroke period then varies as the first power of scale.

These results are very important. The time scale of electrical phenomena (including losses) varies as the square of physical scale, while the time scale of mechanical phenomena (i.e., the fundamental operating time of the system) varies as the first power of scale. As the scale of the system is increased, the time required to complete a fundamental energy conversion operation (the stroke time) occupies a smaller and smaller fraction of the time required to dissipate a given portion of the stored energy. Qualitatively, then, the free- piston generator system becomes more electrically efficient as the physical scale is increased.

An exact quantitative expression of the dependence of efficiency on scale requires case-by-case numerical computation. However, a simplified analysis still provides informative results. First, consider the converted output power requirement to be independent of scale. Then the energy conversion required per stroke can be expressed as follows:

$$E_s = Pt_s \qquad \text{(Eq. 15)}$$

where P is the output power and t_s is the stroke time. An approximate expression for the level of power dissipation is

$$P_d = \frac{E_s}{\tau} = P\frac{t_s}{\tau} \qquad \text{(Eq. 16)}$$

where τ represents the time constant. Finally, an expression for the efficiency results:

$$\eta = 1 - \frac{P_d}{P} = 1 - \frac{t_s}{\tau} \qquad \text{(Eq. 17)}$$

Given the previously determined scale dependence of the stroke time and time constant, this result indicates that the fractional dissipation varies as the inverse first power of scale, that is, doubling the size of the system cuts the fractional losses in half. The proof-of-feasibility point

design exhibited approximately 83 percent and has a 6-in. stroke and bore. A 12-in. scale design would exhibit approximately 91.5 percent efficiency, while a 3-in. scale design would exhibit approximately 66 percent efficiency. Of course, variations in the relative size of various components might improve any of these figures, but the determination of suitable changes will require an optimization study rather than a simple scaling analysis.

VII. SUMMARY AND RECOMMENDATIONS

The objective of this program was to evaluate the feasibility of a free-piston engine coupled to a linear generator to serve as an auxiliary power unit for a hybrid vehicle. Computer- modeling techniques were used to screen different designs for the linear generator. For this program, five different concepts were evaluated. These concepts included permanent magnet generators, reluctance generators, and two- and three-coil induction generators. The efficiency of the linear generator was highly dependent on the design concept. The two-coil induction generator was determined to be the best design, with an efficiency of approximately 90 percent.

The efficiency of the two-coil generator was improved by shaping the profile to the coils to match the piston speed profile. The piston speed, power output, and generator efficiency are complex functions of geometric parameters such as bore and stroke. The linear generator has to be tailored to match the piston speed. Because of the complexity of the problem and the time available for analysis, none of the engine design parameters were varied other than the manifold air pressure or engine power.

Additional modeling efforts should be directed at evaluating the effect of engine parameter (bore and stroke) on the generator design and efficiency.

VIII. LIST OF REFERENCES

1. Swiderski, A., Rueter, F., and Gagne, R.E., "Free Piston Gasifier Studies: Further Development and Use of the Hybrid Simulation," Mechanical Engineering Report ME-240, National Research Council Canada, January 1973.

2. Bobrowsky, A.R., "Stability of Free-Piston Gas Generators," ASME 72-WA/DGP-2, September 1973.

3. Samolewicz, J.J., "Experimental and Analytical Study of a Small Free-Piston Gasifier," ASME 71-DGP-5, February 1972.

4. Braun, A.T., Flynn Jr., and Orsini, J.F., "The Braun Compressor: A Completely Balanced Reciprocating Compressor for Marine, Rail and Industrial Use," SAE Paper No. 860882, May 1986.

5. Sher, E., "Design Considerations of an Airborne Free Piston Compressor," Proc. Instn. Mech. Engrs., **201:D3**, IMechE, 1987.

6. Wallace, F.J., Wright, E.J., and Campbell, J.S., "Future Development of Free Piston Gasifier Turbine Combinations for Vehicle Traction," SAE Paper No. 660132, January 1966.

7. Heintz, R. P., "Theory of Operation of a Free Piston Engine-Pump," SAE Paper No. 859316, 1985.

8. Beachley, N. H. and Fronczak, F. J., "Design of a Free-Piston Engine-Pump," SAE Paper No. 921740, September 1992.

9. Hibi, A., "Hydraulic Free Piston Internal Combustion Engine," *Hydraulic Pneumatic Mechanical Power*, April 1984.

10. Hibi, A. and Kumagai, S., "Hydraulic Free Piston Internal Combustion Engine -- Test Result," *Power*, September 1984.

DISTRIBUTION LIST

Department of Defense

DEFENSE TECH INFO CTR — 12
CAMERON STATION
ALEXANDRIA VA 22314

ODUSD
ATTN: (L) MRM — 1
PETROLEUM STAFF ANALYST
PENTAGON
WASHINGTON DC 20301-8000

ODUSD
ATTN: (ES) CI — 1
400 ARMY NAVY DR
STE 206
ARLINGTON VA 22202

HQ USEUCOM
ATTN: ECJU L1J — 1
UNIT 30400 BOX 1000
APO AE 09128-4209

US CINCPAC
ATTN: J422 BOX 64020 — 1
CAMP H M SMITH
HI 96861-4020

DIR ADV RSCH PROJ AGENCY
ATTN: ARPA/ASTO — 1
3701 N FAIRFAX DR
ARLINGTON VA 22203-1714

Department of the Army

HQDA
ATTN: DALO TSE — 1
DALO SM — 1
PENTAGON
WASHINGTON DC 20310-0103

SARDA
ATTN: SARD TL — 1
PENTAGON
WASHINGTON DC 20310-0103

CDR AMC
ATTN: AMCRD S — 1
AMCRD IM — 1
AMCRD IT — 1
5001 EISENHOWER AVE
ALEXANDRIA VA 22333-0001

CDR ARMY TACOM
ATTN: AMSTA IM LMM — 1
AMSTA IM LMB — 1
AMSTA IM LMT — 1
AMSTA TR NAC — 1
AMSTA TR R — 1
AMSTA TR M — 1
AMSTA TR M (R MUNT) — 1
AMCPM ATP — 1
AMSTA TR E — 1
AMSTA TR K — 1
AMSTA IM MM — 1
AMSTA IM MT — 1
AMSTA IM MC — 1
AMSTA GTL — 1
USMC LNO — 1
AMCPM LAV — 1
AMCPM M113/M60 — 1
AMCPM CCE/SMHE — 1
WARREN MI 48397-5000

DEPARTMENT OF THE ARMY
MOBILITY TECH CTR BELVOIR
ATTN: AMSTA RBF (M E LEPERA) — 10
AMSTA RBXA (R E TOBEY) — 1
10115 GRIDLEY RD STE 128
FT BELVOIR VA 22060-5843

CECOM-SOUTH
ATTN: AMSEL RD C2 PP P — 1
AMSEL RD C2 PP PA — 1
10108 GRIDLEY RD STE 1
FT BELVOIR VA 22060-5815

PROG EXEC OFFICER
ARMORED SYS MODERNIZATION
ATTN: SFAE ASM S — 1
SFAE ASM BV — 1
SFAE ASM CV — 1
SFAE ASM AG — 1
CDR TACOM
WARREN MI 48397-5000

PROG EXEC OFFICER
ARMORED SYS MODERNIZATION
ATTN: SFAE ASM FR — 1
SFAE ASM AF — 1
PICATINNY ARSENAL NJ 07806-5000

PROG EXEC OFFICER
COMBAT SUPPORT
ATTN: SFAE CS TVL — 1
SFAE CS TVM — 1
SFAE CS TVH — 1
CDR TACOM
WARREN MI 48397-5000

PROG EXEC OFFICER
ARMAMENTS
ATTN: SFAE AR HIP 1
SFAE AR TMA 1
PICATINNY ARSENAL NJ 07806-5000

PROG MGR
UNMANNED GROUND VEH
ATTN: AMCPM UG 1
REDSTONE ARSENAL AL 35898-8060

DIR
ARMY RSCH LAB
ATTN: AMSRL CP PW 1
2800 POWDER MILL RD
ADELPHIA MD 20783-1145

VEHICLE PROPULSION DIR
ATTN: AMSRL VP (MS 77 12) 1
NASA LEWIS RSCH CTR
21000 BROOKPARK RD
CLEVELAND OH 44135

CDR AMSAA
ATTN: AMXSY CM 1
APG MD 21005-5071

CDR ARO
ATTN: AMXRO EN (D MANN) 1
RSCH TRIANGLE PK
NC 27709-2211

CDR AEC
ATTN: SFIM AEC ECC (T ECCLES) 1
APG MD 21010-5401

CDR ARMY ATCOM
ATTN: AMSAT R EP (V EDWARD) 1
4300 GOODFELLOW BLVD
ST LOUIS MO 63120-1798

CDR ARMY NRDEC
ATTN: SATNC US (J SIEGEL) 1
SATNC UE 1
NATICK MA 01760-5018

CDR ARMY CRDEC
ATTN: SMCCR RS 1
APG MD 21010-5423

CDR APC
ATTN: SATPC Q 1
SATPC QE (BLDG 85 3) 1
NEW CUMBERLAND PA 17070-5005

PETROL TEST FAC WEST 1
BLDG 247 TRACEY LOC
DDRW
P O BOX 96001
STOCKTON CA 95296-0960

CDR ARMY TECOM
ATTN: AMSTE TA R 1
AMSTE TC D 1
AMSTE EQ 1
APG MD 21005-5006

PROG MGR PETROL WATER LOG
ATTN: AMCPM PWL 1
4300 GOODFELLOW BLVD
ST LOUIS MO 63120-1798

PROG MGM MOBILE ELEC PWR
ATTN: AMCPM MEP 1
7798 CISSNA RD STE 200
SPRINGFIELD VA 22150-3199

CDR
ARMY COLD REGION TEST CTR
ATTN: STECR TM 1
STECR LG 1
APO AP 96508-7850

CDR
ARMY BIOMED RSCH DEV LAB
ATTN: SGRD UBZ A 1
FT DETRICK MD 21702-5010

CDR FORSCOM
ATTN: AFLG TRS 1
FT MCPHERSON GA 30330-6000

CDR TRADOC
ATTN: ATCD SL 5 1
INGALLS RD BLDG 163
FT MONROE VA 23651-5194

ARMY COMBINED ARMS SPT CMD
ATTN: ATCL CD 1
ATCL MS 1
FT LEE VA 23801-6000

CDR ARMY AVIA CTR
ATTN: ATZQ DOL M 1
ATZQ DI 1
FT RUCKER AL 36362-5115

CDR ARMY CACDA
ATTN: ATZL CD 1
FT LEAVENWORTH KA 66027-5300

CDR ARMY CSTA
ATTN: STECS EN 1
STECS LI 1
STECS AE 1
STECS AA 1
APG MD 21005-5059

CDR ARMY YPG
ATTN: STEYP MT TL M 1
YUMA AZ 85365-9130

CDR ARMY CERL
ATTN: CECER EN 1
P O BOX 9005
CHAMPAIGN IL 61826-9005

DIR 1
AMC FAST PROGRAM
10101 GRIDLEY RD STE 104
FT BELVOIR VA 22060-5818

Department of the Navy

DIR LOGISTICS PLANS & POLICY/
STRATEGIC SEALIFT PROG DIV (N42)
ATTN: N420 1
2000 NAVY PENTAGON
WASHINGTON DC 20350-2000

CDR
NAVAL SEA SYSTEMS CMD
ATTN: SEA 03M3 1
2531 JEFFERSON DAVIS HWY
ARLINGTON VA 22242-5160

CDR
NAVAL SURFACE WARFARE CTR
ATTN: CODE 63 1
CODE 632 1
CODE 859 1
3A LEGGETT CIRCLE
ANNAPOLIS MD 21402-5067

CDR
NAVAL RSCH LABORATORY
ATTN: CODE 6181 1
WASHINGTON DC 20375-5342

CDR
NAVAL AIR WARFARE CTR
ATTN: CODE PE33 AJD 1
P O BOX 7176
TRENTON NJ 08628-0176

CDR
NAVAL AIR SYSTEMS CMD
ATTN: AIR 53623C 1
1421 JEFFERSON DAVIS HWY
ARLINGTON VA 22243-5360

Department of the Navy/U.S. Marine Corps

HQ USMC
ATTN: LPP 1
WASHINGTON DC 20380-0001

PROG MGR COMBAT SER SPT 1
MARINE CORPS SYS CMD
2033 BARNETT AVE STE 315
QUANTICO VA 22134-5080

PROG MGR GROUND WEAPONS 1
MARINE CORPS SYS CMD
2033 BARNETT AVE
QUANTICO VA 22134-5080

PROG MGR ENGR SYS 1
MARINE CORPS SYS CMD
2033 BARNETT AVE
QUANTICO VA 22134-5080

CDR
MARINE CORPS SYS CMD
ATTN: SSE 1
2030 BARNETT AVE STE 315
QUANTICO VA 22134-5010

Department of the Air Force

HQ USAF/LGSSF
ATTN: FUELS POLICY 1
1030 AIR FORCE PENTAGON
WASHINGTON DC 20330-1030

HQ USAF/LGTV
ATTN: VEH EQUIP/FACILITY 1
1030 AIR FORCE PENTAGON
WASHINGTON DC 20330-1030

AIR FORCE WRIGHT LAB
ATTN: WL/POS 1
WL/POSF 1
1790 LOOP RD N
WRIGHT PATTERSON AFB
OH 45433-7103

SA ALC/SFT 1
1014 BILLY MITCHELL BLVD STE 1
KELLY AFB TX 78241-5603

Other Federal Agencies

NASA
LEWIS RESEARCH CENTER 1
CLEVELAND OH 44135

NIPER
PO BOX 2128 1
BARTLESVILLE OK 74005

DOE
CE 151 (MR RUSSELL) 1
1000 INDEPENDENCE AVE SW
WASHINGTON DC 20585

Other

DR WILLIAM WELDON 1
CENTER FOR ELECTROMECHANICS
PICKLE RESEARCH CENTER
10100 BURNET ROAD
AUSTIN TX 78758-4497